ESO Science Archive Facility - Phase 3 Data Release Description
ESO programme M33 Muse, Data Release IN PROGRESS
provided by Anna Feltre, published on 2026-06-03

M³D: Mosaicking M33 with MUSE

Unveiling the diversity of H II regions in M33 with MUSE

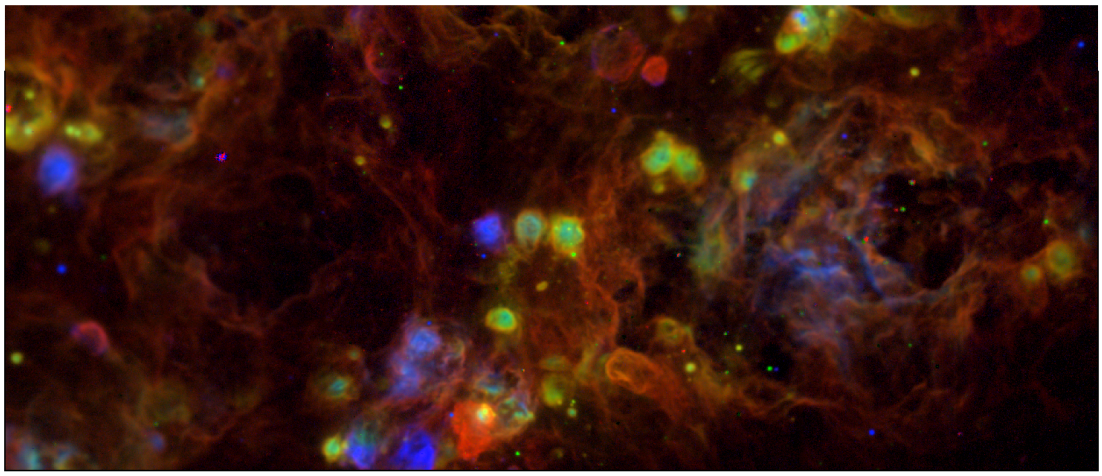

Abstract

We present the public release of VLT/MUSE integral field spectroscopy observations of a 3′ × 8′ mosaic along the southern major axis of the Local Group spiral galaxy M33, obtained under ESO Programme 109.22XS.001 (PI: G. Cresci). The observations were carried out in seeing-limited wide-field mode (WFM), covering the nominal wavelength range 4750 and 9350 Å. The final mosaic comprises 24 pointings, corresponding to a total sky coverage of ∼24 arcmin^2 (∼1.43 kpc^2 at the distance of M33), with a spatial sampling of 0.2″ per pixel (≈0.8 pc physical scale). The released products include fully reduced and flux-calibrated datacubes and emission-line maps. This release enables spatially resolved studies of ionised gas and stellar feedback at parsec scales in a nearby spiral galaxy.
The dataset has been used to identify and characterise 131 H II regions within the mosaic footprint through dendrogram analysis. The data products and the associated nebular catalogue, including integrated emission-line fluxes and derived physical properties, are presented in Feltre et al. (2026).

Overview of Observations

The observations were acquired with MUSE at VLT UT4 in WFM (1′×1′ field of view per pointing, 0.2″ spatial sampling) over the nominal wavelength range 4750–9350 Å. The dataset consists of a mostly contiguous 3' × 8' mosaic of 24 individual MUSE pointings, with an overlap of about 2″ between adjacent fields. Each pointing was observed with two 340 s exposures, with 90° rotation. Dedicated sky exposures (120 s) were obtained after each observing block. Observations were executed between 4 September and 5 October 2022 under seeing conditions typically between 0.6″ and 1.0″, with one observing block obtained under ∼1.5″ seeing conditions. The mosaic covers two spiral arms and an inter-arm region of M33 along its southern major axis. The physical scale, at the adopted distance of M33 of 840 kpc, corresponds to 4.0 pc per arcsecond. Figure 1 shows the position of each individual pointing on top of g – r – i SDSS image.

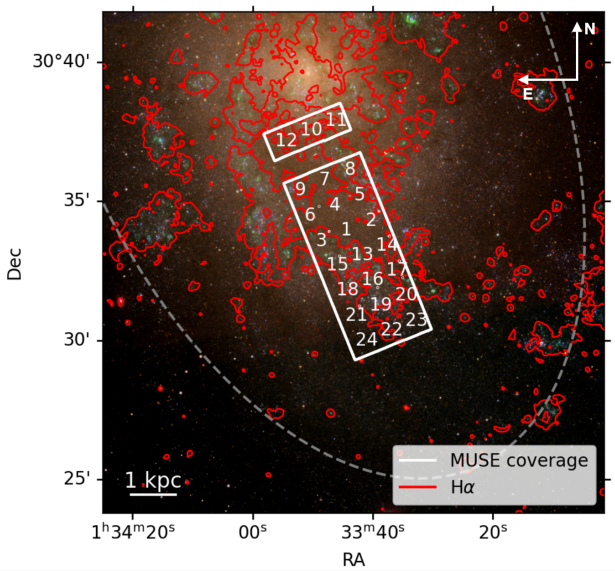

Figure 1. *g -- r --i SDSS image of M33 showing the 24 MUSE pointings.*

Release Content

The release include reduced and calibrated M³D datacubes and emission-line maps. Details are provided below.

Reduced and calibrated mosaic of MUSE datacubes

The mosaic covers 24 arcmin² along the major axis of M33 (Figure 1). Table 1 describes the observing strategy. Each Observing Block (OB) consists of 3 pointings. There is a gap in coverage of approximately one arcmin width between the top set of three pointings and the rest of the mosaic.

Table 1. Observing Log of the MUSE observations for M33

Pointing	RA hms	DEC dms	Obs. date	PSF ″
1-3	01:33:44.273	30:33:54.770	06/09/22	0.5
4-6	01:33:45.956	30:34:48.550	19/09/22	1.0
7-9	01:33:47.638	30:35:42.327	20/09/22	1.5
10-12	01:33:51.005	30:37:29.879	04/09/22	0.7
13-15	01:33:42.591	30:33:00.999	25/09/22	0.7
16-18	01:33:40.909	30:32:07.221	29/09/22	0.9
19-21	01:33:39.230	30:31:13.444	03/10/22	0.8
22-24	01:33:37.547	30:30:19.667	05/10/22	1.0

Notes. Each row corresponds to one OB observed on the same night within a 1 hour interval. The table includes pointing numbers corresponding to the OB (column 1, see Fig. 1), pointing centre of the middle pointing of the strip (columns 2 and 3), data of observation (column 4), estimate of the seeing from the observatory DIMM monitor (column 5).

Emission-line maps

The data product consists of a multi-extension FITS file containing 204 two-dimensional maps. A simplified overview of the extension structure is provided in Table 2, while the complete list of extensions can be retrieved from the `EXTNAME` and `BUNIT` keywords of the FITS file. Among the available products, the maps most extensively used in Feltre et al. (2026) are those of Hβ λ4861, [O III] λ4959,5007, Hα λ6562, [N II] λ6548,6584, [S II] λ6716,6731, and [S III] λ9069 emission-line fluxes. Maps are continuum-subtracted, corrected for Milky Way foreground extinction, and derived via spaxel-by-spaxel spectral fitting. All extensions contain images with identical spatial dimensions.

Table 2. Synthetic description of the emission-line maps data product.

Extension	Units	Description
ID	–	Spaxel identification number map.
FLUX	10^{-20} erg s^{-1} cm^{-2} spaxel^{-1}	Stellar continuum flux map
SNR	–	Signal-to-noise ratio measured per spaxel.
SNRBIN	–	Signal-to-noise ratio measured per Voronoi bin.
BIN_ID	–	Voronoi bin identification map.
V_STARS	km s^{-1}	Stellar line-of-sight velocity.
FORM_ERR_V_STARS	km s^{-1}	Formal uncertainty on the stellar velocity.
SIGMA_STARS	km s^{-1}	Stellar velocity dispersion.
FORM_ERR_SIGMA_STARS	km s^{-1}	Formal uncertainty on the stellar velocity dispersion.
H3_STARS	–	Gauss–Hermite moment h_3.
FORM_ERR_H3_STARS	–	Formal uncertainty on h_3.
H4_STARS	–	Gauss–Hermite moment h_4.
FORM_ERR_H4_STARS	–	Formal uncertainty on h_4.
BIN_ID_GAS	–	Voronoi bin identification map.
CHI2_TOT	–	Total χ^2 of the stellar spectral fit.
HB4861_FLUX	10^{-20} erg s^{-1} cm^{-2} spaxel^{-1}	Integrated flux of the Hβ emission line.
HB4861_FLUX_ERR	10^{-20} erg s^{-1} cm^{-2} spaxel^{-1}	Uncertainty on the Hβ flux.
HB4861_VEL	km s^{-1}	Line-of-sight velocity measured the Hβ.
HB4861_VEL_ERR	km s^{-1}	Uncertainty on the Hβ velocity.
HB4861_SIGMA	km s^{-1}	Observed velocity dispersion of Hβ.
HB4861_SIGMA_ERR	km s^{-1}	Uncertainty on the observed Hβ velocity dispersion.
HB4861_SIGMA_CORR	km s^{-1}	Velocity dispersion corrected for instrumental broadening.
⋮		emission-line maps (flux, velocity, dispersion, and associated uncertainties) are provided for various trantitions and can be retrieved using the EXTNAME keyword.
SIII9068_SIGMA_CORR	km s^{-1}	Instrumental-resolution corrected velocity dispersion of the [SIII] λ9068 emission line.

Release Notes

The data were reduced using pymusepipe (Emsellem et al. 2022), a Python wrapper around the ESO MUSE data reduction pipeline (Weilbacher et al. 2020). Standard MUSE pipeline recipes were applied to remove instrumental signatures, including bias subtraction, flat-fielding, illumination correction, wavelength

calibration, line spread function determination, and flux calibration using spectrophotometric standard stars. All wavelengths are air wavelengths.

Astrometric alignment and refinement of the absolute flux calibration were performed using an SDSS r-band mosaic of the same field as reference. Individual exposures were aligned using the optical-flow tool spacepylot, and multiplicative flux corrections were derived from a linear regression between reconstructed MUSE r-band images and the SDSS reference image. The final data product is a flux-calibrated mosaic cube combining the 24 MUSE pointings. Emission-line maps were derived from the final mosaic using spectral fitting procedures based on pPXF, as described below.

Data Reduction and Calibration

Mosaic of datacubes

Dedicated offset sky exposures were used to construct sky spectra for subtraction. Since the science fields are fully embedded within M33, these dedicated sky frames were essential to ensure reliable background removal.

To refine the absolute flux calibration and improve the sky subtraction, a linear regression was performed between the reconstructed MUSE r-band flux and the SDSS reference image in 3″ × 3″ bins. The slope of this relation was applied as a multiplicative correction to the flux normalisation of each exposure, while the intercept was used to correct residual background offsets (see Emsellem et al. 2022, Sec. 4.2.5).

The final mosaic was produced by combining the 48 individual exposures (two per pointing) onto a common astrometric grid.

Spectral fitting and Emission line maps

Emission-line maps were derived from the final mosaic datacube using the PHANGS data analysis pipeline, based on pPXF (Cappellari & Emsellem 2004; Cappellari 2017). Prior to fitting, the data were corrected for foreground Galactic extinction using the O'Donnell (1994) extinction law and the Schlafly & Finkbeiner (2011) reddening value for M33.

The stellar continuum was first fitted on Voronoi-binned data with a target signal-to-noise ratio of 35 in the continuum around 5400 Å, using E-MILES simple stellar population templates (Vazdekis et al. 2016) to derive the stellar kinematics. Emission lines were then fitted at the level of individual spaxels, keeping the stellar kinematics fixed to those of the corresponding Voronoi bin.

The released maps include Hβ λ4861, [O III] λ4959,5007, [N II] λ6548,6584, Hα λ6562, [S II] λ6716,6731, and [S III] λ9069. Emission lines were modelled as Gaussian components, with kinematic parameters tied in groups (Balmer, low-ionisation, and high-ionisation lines), and theoretical flux ratios enforced for doublets such as [O III] and [N II]. The emission-line maps are continuum-subtracted and corrected for Milky Way foreground extinction.

Data Quality

Astrometry

The astrometric solution of the MUSE mosaic is tied to the SDSS r-band reference image used during the alignment procedure. Individual exposures were aligned using the optical-flow based routine *spacepylot*, correcting for both translational and rotational offsets. Before correction, absolute offsets with respect to SDSS were typically of order 1.5″ (up to 2.5″). After alignment, relative offsets between exposures are comparable to the MUSE pixel scale (0.2″).

Spatial resolution

The spatial resolution varies across the mosaic depending on the seeing conditions of each observing block (Table 1). Most observations were obtained under seeing between 0.6″ and 1.0″, with one observing block reaching ~1.5″. At the adopted distance of M33 (840 kpc), 1″ corresponds to 4 pc, resulting in a physical resolution of approximately 2–6 pc across the dataset.

Known issues

Residual sky-line features may affect portions of the reddest wavelength range, particularly near strong atmospheric emission lines. These residuals primarily impact weak lines and do not significantly affect the main emission lines included in the released maps.

Previous Releases

N/A

Data Format

Files Types

The primary data product of this release is the mosaicked MUSE datacube:

- **`M33_cube.fits`** Multi-extension FITS file containing the data extension (EXTNAME=DATA), the variance extension (EXTNAME=STAT) and the data quality extension (EXTNAME=DQ). The datacubes of the 24 individual pointings are not included in this release.

The release is accompanied by the following ancillary products:

- **`M33_MAPS.fits`** Emission line maps. A multi-extension FITS file containing all the quantities derived from fitting the datacube with pPXF. Table 2 above describes the included extensions.
- **`M33_whitelight.fits`** A white-light image obtained by averaging the datacube across all available wavelengths.

All files are provided in standard ESO Phase 3 FITS format.

Catalogue Columns

N/A

Acknowledgements

According to the Data Access Policy for ESO data held in the ESO Science Archive Facility, all users are required to acknowledge the source of the data with an appropriate citation in their publications.

Since processed data downloaded from the ESO Archive are assigned Digital Object Identifiers (DOIs), the following statement must be included in all publications making use of them:

Based on observations collected at the European Southern Observatory under ESO programme 109.22XS.001.

The dataset and data reduction associated with this data release is described in detail in Feltre et al., 2026 (A&A 706, A367). Please cite this paper when making use of this dataset. The paper is available at the following link: https://www.aanda.org/articles/aa/full_html/2026/02/aa57122-25/aa57122-25.html

Science data products from the ESO archive may be distributed by third parties, and disseminated via other services, according to the terms of the Creative Commons Attribution 4.0 International license. Credit to the ESO provenance of the data must be acknowledged, and the file headers preserved.

References

Cappellari, M., & Emsellem, E. 2004, PASP, 116, 138
Cappellari, M. 2017, MNRAS, 466, 798
Emsellem, E., et al. 2022, A&A, 659, A191
Feltre, A., et al. 2026, A&A, 706, A367
O'Donnell, J. E. 1994, ApJ, 422, 158
Schlafly, E. F., & Finkbeiner, D. P. 2011, ApJ, 737, 103
Vazdekis, A., et al. 2016, MNRAS, 463, 3409
Weilbacher, P. M., et al. 2020, A&A, 641, A28